

Large-scale Valorization of Bauxite Residue for Inorganic Polymers

Tobias Hertel¹, Remus Ion Iacobescu², Bart Blanpain³ and Yiannis Pontikes³

1. Research Associate,

2. Senior Researcher,

3. Professor

KU Leuven, Department of Materials Engineering, Kasteelpark Arenberg 44, 3001 Leuven, Belgium

Corresponding author: Tobias.Hertel@kuleuven.be

Abstract

A process is suggested in this paper to valorize bauxite residue (BR) on a large-scale. The resulting material is a binder that can be used, depending on its properties, in the production of bricks and tiles, or as an aggregate which can be safely stored in landfills or used in concrete or asphalt. The strategy is to develop a precursor that upon mixing with alkalis will lead to an inorganic polymer. To achieve the above, thermodynamic calculations were carried out. It was found that reducing conditions and additional silica promote the formation of an Fe²⁺-rich liquid phase during heating, which is expected to result in an amorphous phase upon solidification. In practice, this implies minor additions of silica and carbon to the bauxite residue, and firing at temperatures of about 1200 °C to produce a semi-glassy precursor. Experimental work verified the above hypothesis and indeed a highly reactive alkali activated binder was formed. Mixing this binder with “fresh” filter-pressed BR at a ratio 3:7 led to a hard, water-insoluble, reddish composite that can find different applications. An industrial implementation seems to be straightforward since existing installations can be adapted and only minor additions have to be carried out.

Keywords: Bauxite Residue; valorization; inorganic polymer; aggregate; firing.

1. Introduction

Bauxite residue (BR), also referred to as ‘red mud’, is generated during the digestion of bauxite in the Bayer process, exceeding a yearly production of 150 Mt [1]. The global inventory of BR is estimated to be above 2.7 Gt in 2007 [2]. BR is still considered as a problematic waste stream of alumina production, and as a result, one of the potential uses of it entails incorporating it in existing industrial processes. The main driving forces for the valorization of BR are the lack of storage volume in the disposal areas, as well as the long-term liability such storing incurs. The composition of BR with substantial amounts of Fe₂O₃, Al₂O₃, TiO₂ and critical minor elements makes it attractive as a raw material for the recovery of valuable major metals or rare earth elements (like scandium) [3,4] but also in ceramics [5] or in building materials [6].

In addition to the use of BR as source for Al and Fe in ordinary Portland cements (OPC) or in low-energy binders, such as calcium sulfoaluminate (CSA) cements, attempts have been made to valorize BR in inorganic polymers (IP). The strength development of these alternative cementitious binders is based on polymerization reactions in alkaline media [7]. BR has been used in IP binder systems in combination with reactive materials such as metakaolin [8] or ground granulated blast furnace slag (GGBFS) [9]. Generally, an addition of BR to these reactive precursor materials leads to decreasing properties of the binder, with the result that the BR fraction in these binders is kept low to reach satisfying mechanical properties. Chemical and also partially thermal modifications of BR have been carried out by Hairi et al. who transformed it into a reactive material by using raw or tempered (500 °C) BR and mixing it with different additions like amorphous silica fume (6-26 wt%) and alumina (0-20 wt%) [10].

In contrast to the presented studies, the aim of this work is to use as much as BR as possible without using costly additives or other reaction promoters. The concept is to thermally and chemically modify BR and create a substantial amount of amorphous phase resembling other non-ferrous slags. It has been shown in the past that non-ferrous slags with a deviation from the traditional aluminosilicate chemistry, for example copper slag, can lead to IP [11]. Main characteristics of these iron-rich precursors is iron in oxidation state +II and with a high amorphous fraction [12]. The chemistry of BR is comparable with other iron-rich precursors, however the degree of crystallinity differs. Also, most of the iron in BR is trivalent. In the present work a process is presented which aims at a large-scale valorization of BR into a novel construction material. The focus of the study is whether a modified BR has the potential to form an inorganic polymer binder, and if that binder combined with fresh BR can deliver a final composite matrix suitable for certain applications.

2. Experimental Methods

2.1. Characterization of the raw material

The starting material of all experiments was filter pressed BR cake, provided by Aluminium of Greece (AoG). BR was dried for 72 h at 105 °C. The chemical composition was determined by semi-quantitative X-ray fluorescence (XRF). Thermogravimetric analysis (TGA) was performed up to 1000 °C using a heating rate of 5 °C/min in Ar atmosphere to determine thermal behavior. The mineralogy was determined by quantitative X-ray diffraction analysis (QXRD). The procedure is described elsewhere [13].

2.2. Thermodynamic calculations

The thermochemical software FactSage 7.0 was used in combination with the FACTPS (pure substances), FToxid (oxide compounds/solutions) and FSstel (steel intermetallic compounds/steel alloy solutions) databases. The focus of the thermodynamic calculations was on the development of a liquid phase fraction during a heat treatment to 1200 °C by adding varying amounts of carbon (to reduce the predominant Fe³⁺ originating from hematite into Fe²⁺) and silica in a mix with BR. As an alternative to silica, different calcia additions were modeled. In industrial practice, silica and calcia correspond to sand and limestone additions, which are easily available, low-cost resources.

2.3. Modification of BR

Based on the results of the thermodynamic calculations (FactSage), a mix of BR, carbon (graphite powder) and silica (microcrystalline SiO₂) in a weight ratio of 88.56:1.44:10 was mixed for 10 hours. Subsequently, firing was performed in a closed alumina crucible using an induction furnace with a SiC external crucible as susceptor. The atmosphere in the crucible was kept inert by flushing Ar (60 l/h) through a gas inlet which was integrated in the crucible lid. The forming gas species were released via a gas outlet. The sample was heated with a heating rate of 5 °C/min, followed by an isothermal step of 1 h at a maximum temperature of 1200 ± 30 °C. To suppress crystallization of the liquid phase during solidification, the semi-molten slag was quenched in water by tilting the furnace. The obtained precursor ('Pr_A') was dried at 105 °C until a constant weight was reached.

2.4. Characterization of the precursor

After drying, the precursor was milled for 5 min. The chemical composition was determined using semi-quantitative XRF. The true density was determined as well as the specific surface area according to EN 196-6 (Blaine method). For microchemical analysis of the crystalline and amorphous fractions an electron probe microanalyzer was employed (EPMA WDS). For this, the powdered precursor was embedded in epoxy resin, followed by polishing and coating with a 30 nm carbon layer. Additionally, for morphologic investigations a scanning electron microscope (SEM) was used on a duplicate sample coated with 1 nm Pt. Attenuated total reflectance Fourier transform infrared spectroscopy (ATR-FTIR) was employed for structural characterization.

2.5. Synthesis of inorganic binders

Two different types of inorganic binder (IB) were synthesized. The first type ('IB_A') consists of 100 % Pr_A as solid precursor. Inorganic binder samples were prepared by mixing the precursor with activation solution (molar ratios $\text{SiO}_2/\text{Na}_2\text{O} = 1.6$ and $\text{H}_2\text{O}/\text{Na}_2\text{O} = 16$) according to an activator to solid weight ratio of 0.15. Preliminary tests have shown that a higher ratio results in squeezing out the paste during pressing. Homogenization was carried out using a hand mixer for 5 min in total. Formed agglomerates were broken manually with a spatula. The samples were shaped (dimensions $2 \times 2 \times 8 \text{ cm}^3$) using an automatic hydraulic press. A constant force of 49 MPa was applied to the sample for 1 min. The choice of pressing the samples for shaping not only leads to a minimum activation solution requirement, but also to a low degree of porosity. The pressed samples were then cured at 60 °C for 48 h. After the envisaged curing time, the curing oven was cooled down slowly to 20 °C to avoid cracking. To check whether the inorganic polymers produced are insoluble or not, specimens of the synthesized products were immersed in hot water (constant 60 °C) for 48 h. The same IB preparation method was repeated for the second sample type, a two component solid mix consisting of filter-pressed, 'fresh' bauxite residue and Pr_A in a 70/30 weight ratio ('IB_B'). The same activation solution was used as for IB_A, however a higher activator to precursor ratio of 0.2 was chosen.

2.6. Characterization of IB

Mechanical properties of the resulting IBs were measured after 3 days of curing using an Instron 5985 testing machine (100 kN cell load). A crosshead speed of 2 mm/min was used for compressive strength testing and 0.5 mm/min for determining the flexural strength. ATR-FTIR was used for structural characterization. SEM and EPMA WDS measurements were carried out for morphological and microchemical analysis on cut and polished specimens.

3. Results and Discussion

3.1 Characterization of BR

The normalized, semi-quantitative XRF result of BR is displayed in Table 1. The loss on ignition (L.O.I.), determined by TGA, is included in the data.

Table 1. Semi-quantitative, normalized XRF data and L.O.I. of used BR (estimated relative error 10%).

Oxide	Fe ₂ O ₃	Al ₂ O ₃	CaO	SiO ₂	TiO ₂	Na ₂ O	Other	L.O.I.
Weight%	47	23	9	9	6	3	<3	11

As minor oxides, MgO (0.3 wt%), Cr₂O₃ (0.3 wt%), V₂O₅ (0.3 wt%) and NiO (0.2 wt%) were detected. The relatively high fraction of Al₂O₃, present in the investigated BR is also reflected in the high amount of Al-containing compounds like diaspore, gibbsite or katoite (Figure 1). Fe is mainly present in the form of hematite (Fe₂O₃).

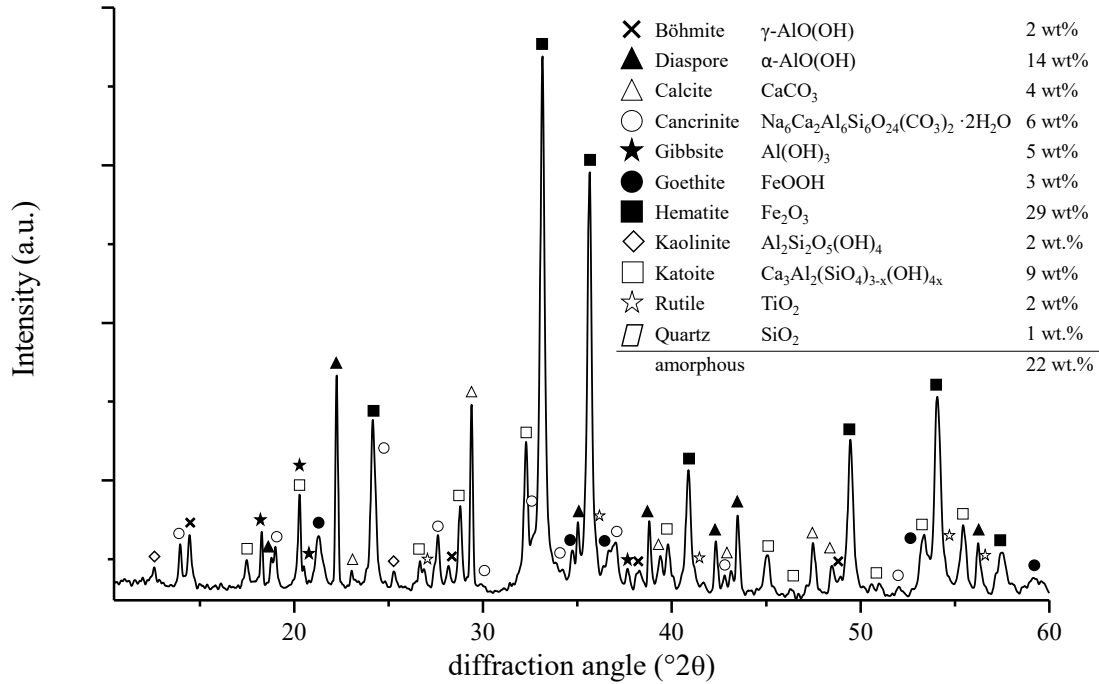


Figure 1. XRD diffractogram of BR including peak identification and Rietveld quantification (estimated relative error 10%).

3.2. Thermodynamic calculations and firing

The results of the thermodynamic calculations (FactSage) at 1200 °C show that increasing carbon and silica additions to BR increase the fraction of liquid phase formed. In Figure 2a the fraction of liquid phase against the carbon content in mix with BR is shown. A maximum quantity of 47 wt% melt is formed in a mix consisting of 98 wt% BR and 2 wt% C. A further increase in carbon content leads to the formation of metallic iron (not shown in the graph) at the expense of lower quantities of formed liquid phase. In Figure 2b a ratio of BR/C = 61.5 is kept constant and different contents of silica or calcia are modeled.

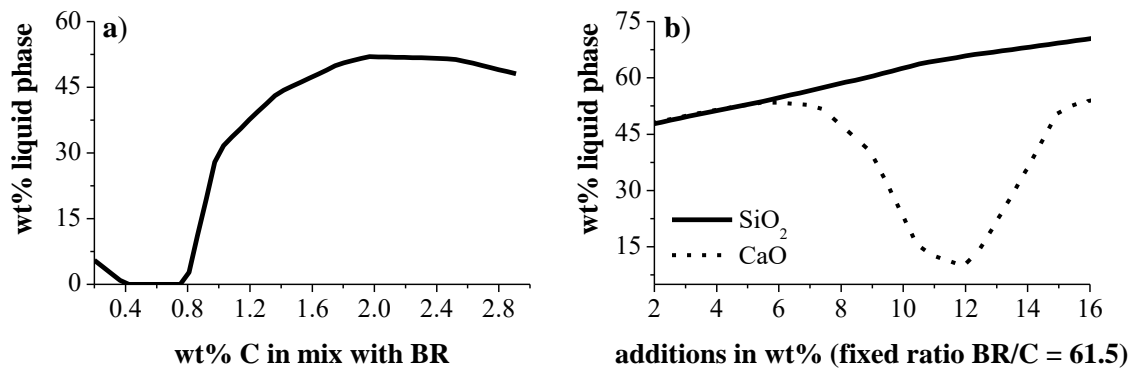


Figure 2. Modeled quantity of liquid phase in wt% (y-axis) at 1200 °C as a function of a) carbon content in a mix with BR and b) silica or calcia content for a fixed ratio of BR/C.

It is shown that increasing silica continuously promotes the formation of liquid phase while calcia increases the quantity of liquid phase formation only up to 7 wt%. A higher content of calcia leads to decreasing liquid phase formation followed by again increasing quantities of liquid phase above 12 wt%. The blend, which was chosen for further experiments, consisted of 88.56 wt% BR, 1.44 wt% C (ratio BR/C = 61.5) and 10 wt% SiO₂. Silica was chosen over CaO because of the lower addition needed for maximizing the liquid phase. The expected phase assemblage at 1200 °C (state of equilibrium) is displayed in Table 2.

Table 2. Modeled phase composition (state of equilibrium) at 1200 °C for Pr_A.

Phase	Spinels			Liquid
	Magnetite Fe ₃ O ₄	Hercynite FeAl ₂ O ₄	Ülvospinel Fe ₂ TiO ₄	
Weight%	11	16	5	67

The composition of the expected liquid phase, expressed in molar ratios, is shown in Table 3.

Table 3. Molar ratios in liquid phase.

SiO ₂ /Al ₂ O ₃	SiO ₂ /FeO	SiO ₂ /CaO
3.2	1.1	2.1

3.3. Characterization of precursor

The recorded XRD diffractogram of Pr_A is displayed in Figure 3.

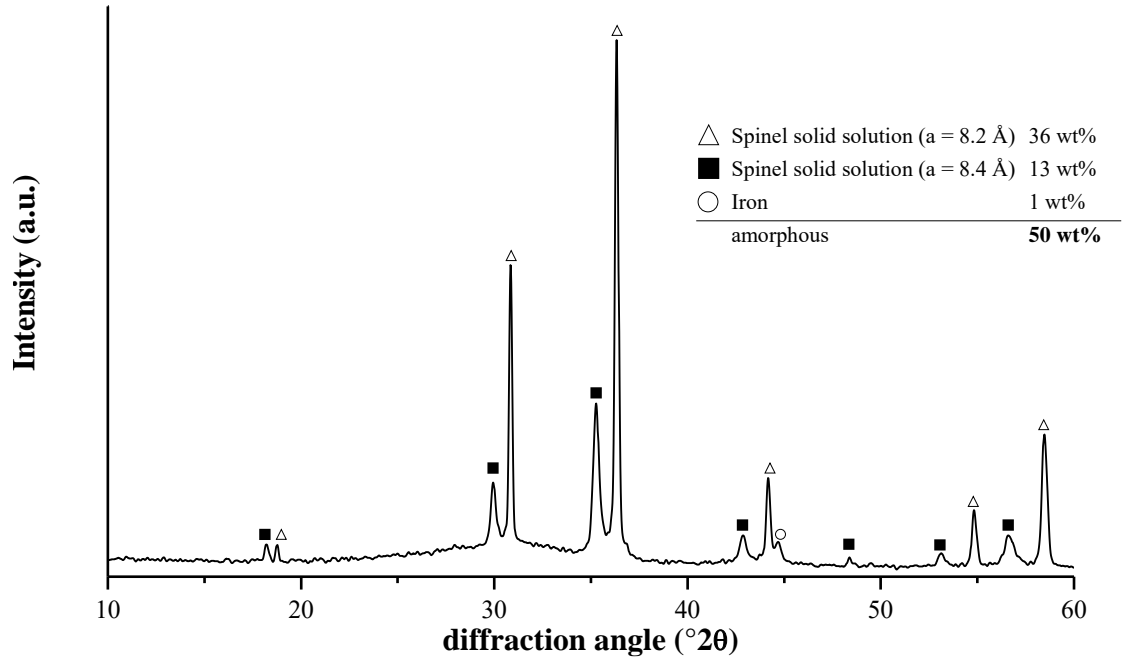


Figure 3. QXRD analysis of Pr_A including peak identification and Rietveld quantification (estimated relative error 10%).

As predicted in the thermodynamic calculations, crystalline spinels, occurring in solid solutions, are formed during firing. Metallic iron was detected as a minor crystalline component. About half of the precursor sample was found amorphous. A possible reason for the deviation in amorphous fraction compared to the expected phase assemblage (based on the calculated liquid fraction) can be explained for instance by the firing time which is assumed not to be sufficient for reaching the state of equilibrium. In addition, no homogenization was carried out during the firing. The formation of metallic iron can be explained by a possible local reduction of Fe^{3+} to Fe^0 . The XRF data of Pr_A are displayed in Table 4.

Table 4. Semi-quantitative XRF data of Pr_A (estimated relative error 10%).

Oxide	Fe _{total}	Al ₂ O ₃	CaO	SiO ₂	TiO ₂	Na ₂ O	Other
Weight%	30	24	8	20	5	2	< 2

The higher amount of alumina in the precursor sample compared to the expected composition can be explained by the influence and interaction of the crucible with the slag, which was not originally saturated in alumina. Further thermodynamic modeling has proven that additional Al₂O₃ slightly decreases the amount of liquid phase at 1200 °C in favor of the formation of Al-rich spinels, which is in accordance with the presented data.

The specific surface area of Pr_A was found to be $5000 \pm 250 \text{ cm}^2/\text{g}$, which is in the range of ordinary Portland cement (e.g. 52.5N). In Figure 4 the structure of a polyphase grain, embedded in resin (black), is displayed.

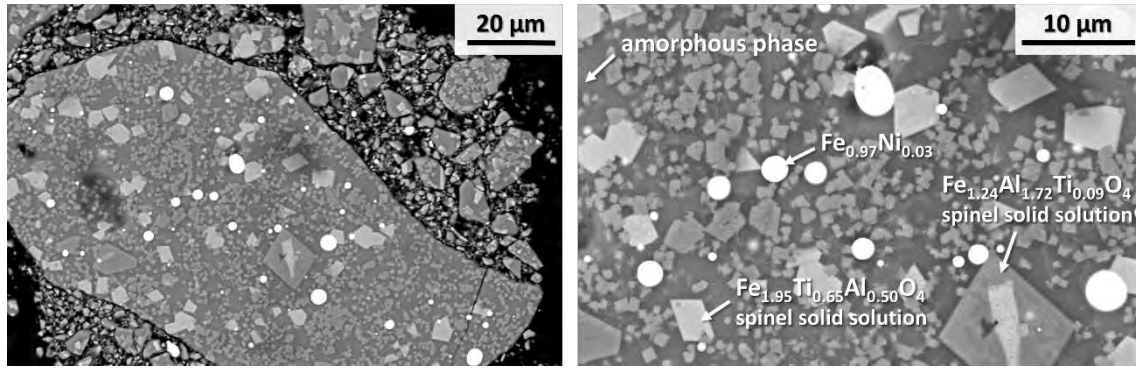


Figure 4. BSE image (SEM) of Pr_A.

The grain structure is characterized by two distinguishable, partially idiomorphic spinel solid solutions, often in parallel growth, as well as iron droplets - doped with Ni - embedded in an amorphous matrix. The size of the crystallites rarely exceeds 10 μm , while the aggregate-like grains show a broad variation in size, exceeding partially 100 μm . The grains are furthermore characterized by sharp, well-defined grain boundaries, most probably a result of the mechanical impact during milling. The molar ratios of the major oxides in the amorphous slag phase are shown in Table 5.

Table 5. Molar ratios of amorphous fraction (derived from EPMA WDS, average of 6 spot analyses).

$\text{SiO}_2/\text{Al}_2\text{O}_3$	SiO_2/FeO	SiO_2/CaO
3.9 ± 0.2	1.6 ± 0.2	1.7 ± 0.1

The amorphous fraction is enriched in silica compared to the calculated ratios (FactSage) of $\text{SiO}_2/\text{Al}_2\text{O}_3$ and SiO_2/FeO . This can be explained by the lower than modeled fraction of amorphous phase and the incorporation of Al and Fe in crystalline spinel solid solutions. Cr_2O_3 is detected with 0.7 wt% in the spinel solid solutions. Chromium in the amorphous fraction is below the limit of quantification. Assuming that the spinel phases remain stable, leaching of chromium can be neglected. A preferred incorporation of rare earth elements like Sc or radioactive thorium in the crystalline or amorphous fraction was not found.

3.4. Characterization of IB

Both synthesized inorganic polymer binder types did not decompose after submersing in water for 48 h. The microstructure of IB_A reveals the formation of a dense, amorphous binder matrix (Figure 5).

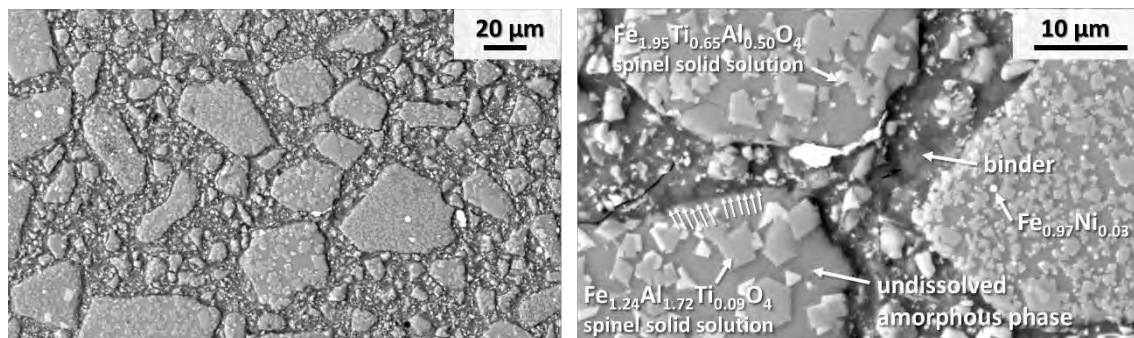


Figure 5. BSE image (EMPA) of IB_A.

The undissolved amorphous fraction, the spinel solid solutions and the metallic iron form aggregates which are connected by an amorphous binder matrix (inorganic polymer matrix). The grain boundaries are characterized by rough edges and dissolution rims (an example is indicated with small arrows in Figure 5, right). An alteration of the spinel minerals was not observed. An indicative composition of the binder phase is listed in Table 6.

Table 6. Indicative molar ratios of binder phase (derived from EPMA WDS, average of 6 spot analyses).

$\text{SiO}_2/\text{Al}_2\text{O}_3$	SiO_2/FeO	SiO_2/CaO
4.0 ± 0.7	1.4 ± 0.1	2.3 ± 0.7

The results shown above can be interpreted as indication of possible incongruent dissolution of the amorphous fraction. Nevertheless, a careful evaluation has to be carried out. Possible vaporization of the sample by the electron beam and an influence of various nanocrystals in the matrix make a definite determination difficult. A possible oxidation of ferrous to ferric iron during polymerization also influences the results. Further work needs to be done to establish the chemical composition of the binder.

Figure 6 shows the microstructure of IB_B, which is characterized by a multitude of fine crystals originating from BR, Pr_A surrounded by an amorphous-like matrix.

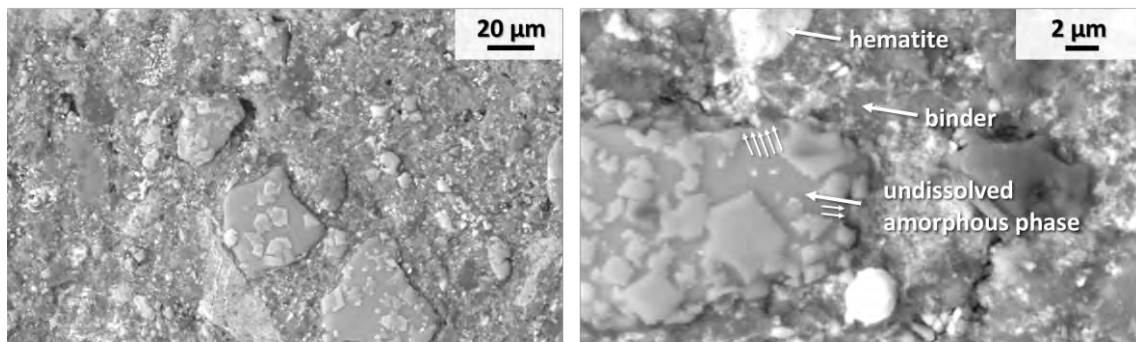


Figure 6. BSE image (EMPA) of IB_B.

The development of a binder can be confirmed, also supported by the occurrence of a dissolution rim (small arrows) of the amorphous phase in the modified BR grain. A quantification of the binder phase is only sporadically possible due to the various minor crystals and amorphous phases (originated from BR). The indicative molar ratios are akin to the ratio of the binder phase in IB_A. The results of FTIR measurement are shown in Figure 7.

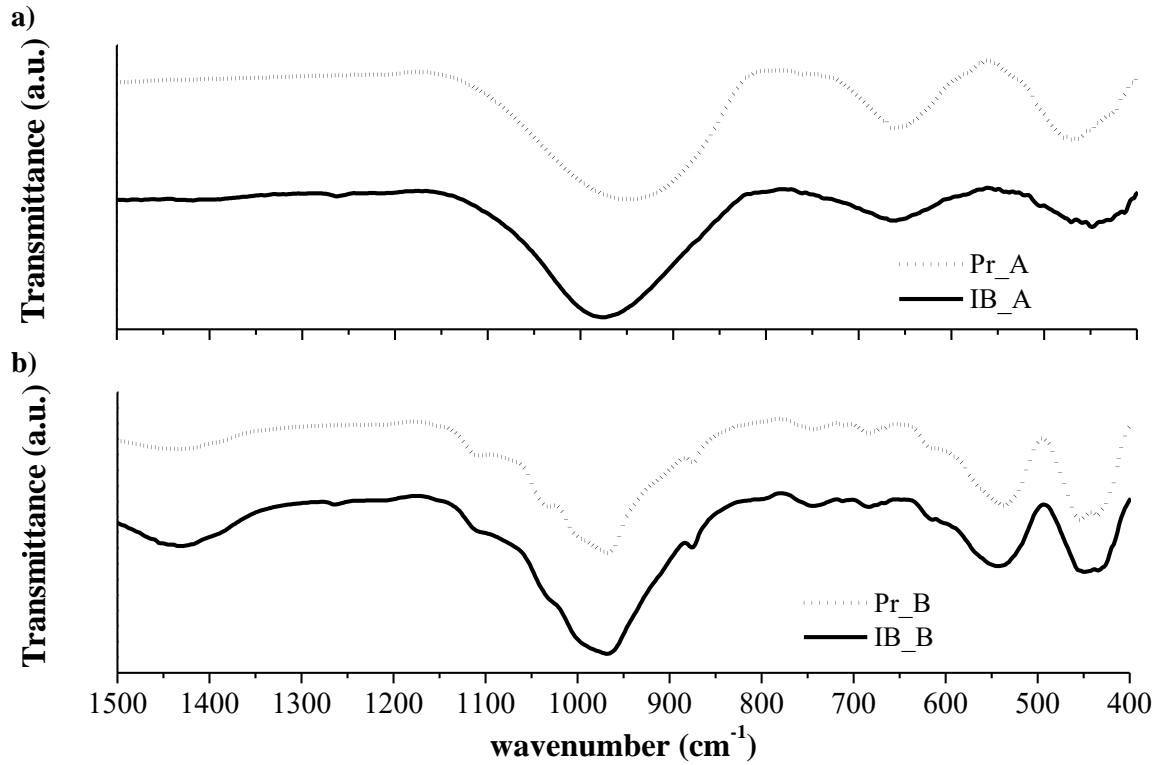


Figure 7. FTIR spectra of a) Pr_A, IB_A and b) Pr_B, IB_B

The focus is on the wavenumber range between 850-1100 cm^{-1} , the region where aluminosilicates show strong asymmetric vibrations of Si-O-T (T = Al, Si) [14,15]. Pure silica glass shows an intensive peak at 1100 cm^{-1} [16]. Due to the incorporation of network modifiers like Fe^{2+} and Ca^{2+} in the present amorphous phase in Pr_A, this peak is shifted to 948 cm^{-1} . After activation of the precursor, the peak is shifted to higher wavenumber (976 cm^{-1}) in IB indicating the formation of a new reaction product with additional silica entering the glassy structure.

Another possible explanation for the shift is the oxidation of Fe^{2+} (network breaker), released by the dissolution of the amorphous phase, to Fe^{3+} (network former) in the formed IB [17]. The differences between precursor and inorganic binder of the sample B are less distinct due to the lower fraction of reactive amorphous phase. Nevertheless, a small relative increase in the intensity of the peak occurring at 980 cm^{-1} supports the hypothesis posed above.

The results of the strength measurements are presented in Table 7. IB_A shows promising values for compressive and flexural strength. Also for IB_B, properties are achieved which suggest the presented materials as candidates for an application in construction, such as tiles or bricks.

Table 7. Mechanical properties of the synthesized products.

Sample	Compressive strength (MPa)	Flexural strength (MPa)
IB_A	149 ± 19	32
IB_B	54 ± 15	16 ± 4

3.5 Possible upscaling

The described path of thermally and chemically modifying BR for the synthesis of inorganic binders seems to be applicable at an industrial scale. Carbon and silica additions can be admixed to a fraction of BR before filter pressing. The produced filter-cake is then thermally processed, e.g. in a rotary kiln, and becomes the reactive precursor. A distinction between BR which is currently produced and BR which is already stored in disposal sites can be made concerning the processing downstream. For the former, the reactive precursor is blended with fresh BR and bricks (Figure 8a), tiles and aggregates can be produced.

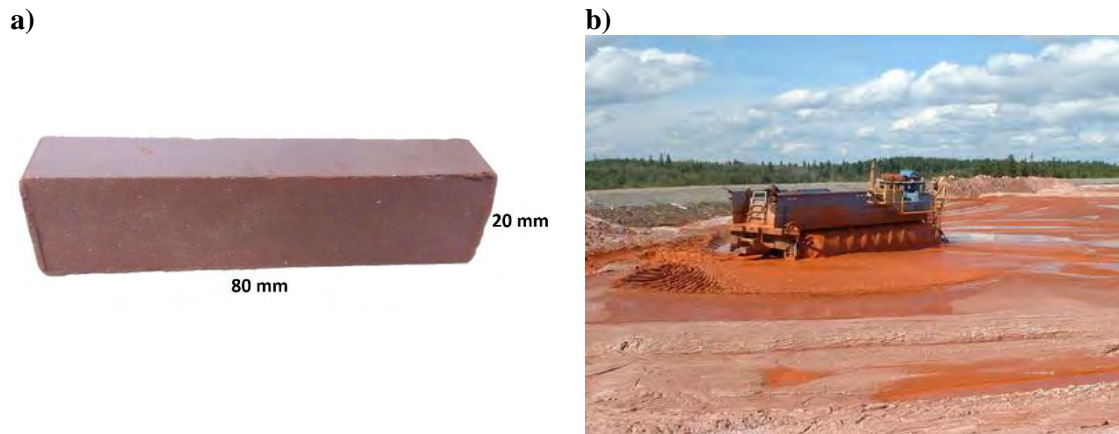


Figure 8. a) Produced brick (IB_B) b) BR farming truck [1].

With respect to disposed BR in legacy sites, the reactive precursor can be spread directly onto BR slurry. Additionally, soluble silicates (e.g. glass or waterglass) can be added and the mix can be homogenized using, for instance, farming trucks (Figure 8b). The mixture is expected to solidify resulting in a dense and hard substrate. This process can turn BR into a safer material to store, more easy also to support revegetation, as part of the alkalis participate in the reaction.

4. Conclusion

In this work a proposal for a large-scale use of BR towards an alternative binder system is presented. It has been demonstrated that dense inorganic binders can be synthesized with promising mechanical properties by modifying a fraction of BR by minor additions of carbon and silica, followed by firing, and finally mixing that reactive precursor with fresh BR. Industrial upscaling seems feasible, where additives, for instance, lignite (carbon source) and sand (silica source) can be used. In that process, it is noteworthy that only a fraction of the BR produced has to be thermally treated.

Acknowledgments

The research leading to these results has received funding from the European Community's Horizon 2020 Programme ([H2020/2014–2019]) under Grant Agreement no. 636876 (MSCA-ETN REDMUD). This publication reflects only the first author's view, exempting the Community from any liability. Project website: <http://www.etn.redmud.org>.

References

1. K. Evans, The History, Challenges, and New Developments in the Management and Use of Bauxite Residue, *Journal of Sustainable Metallurgy*. (2016).
2. C. Klauber, M. Gräfe, and G. Power, Bauxite residue issues: II. options for residue utilization, *Hydrometallurgy*. Vol. 108, No. 1-2, (2011), 11–32.
3. K. Binnemans et al., Towards zero-waste valorisation of rare-earth-containing industrial process residues: A critical review, *Journal of Cleaner Production*. Vol 99, (2015), 17–38.
4. C.R. Borra et al., Leaching of rare earths from bauxite residue (red mud), *Minerals Engineering*. Vol. 76, (2015), 20–27.
5. Y. Pontikes et al., Effect of firing temperature and atmosphere on sintering of ceramics made from Bayer process bauxite residue, *Ceramics International*. Vol. 35, No. 1, (2009), 401–407.
6. Y. Pontikes, G.N. Angelopoulos, Bauxite residue in cement and cementitious applications: Current status and a possible way forward, *Resources, Conservation and Recycling*. Vol. 73, (2013), 53–63.
7. J. Davidovits, Geopolymer chemistry and applications, 3rd ed., Institut Géopolymère, Saint-Quentin, 2011.
8. D.D. Dimas, I.P. Giannopoulou, and D. Panias, Utilization of alumina red mud for synthesis of inorganic polymeric materials, *Mineral Processing and Extractive Metallurgy Review*. Vol. 30, No. 3, (2009), 211–239.
9. N. Ye, J. Yang, and X. Ke, Synthesis and Characterization of Geopolymer from Bayer Red Mud with Thermal Pretreatment, *Journal of American Ceramic Society*. Vol. 97, No. 5, (2014), 1652–1660.
10. S.N.M. Hairi et al., Synthesis and properties of inorganic polymers (geopolymers) derived from Bayer process residue (red mud) and bauxite, *Journal of Material Science*. Vol. 50, No. 23, (2015), 7713–7724.
11. S. Onisei, K. Lesage, and B. Blanpain, Early Age Microstructural Transformations of an Inorganic Polymer Made of Fayalite Slag, *Journal of American Ceramic Society*. Vol. 98, No. 7, (2015) 2269–2277.
12. Y. Pontikes, L. Machiels, and S. Onisei, Slags with a high Al and Fe content as precursors for inorganic polymers, *Applied Clay Science*. Vol. 73, (2013), 93–102.
13. R. Snellings et al., Rietveld Refinement strategy for Quantitative Phase Rietveld Refinement strategy for Quantitative Phase analysis of Partially Amorphous zeolitized tuffaceous rocks, *Geologica Belgica*. Vol 13, No. 3, (2010), 183–196.
14. J.A. Gadsden, Infrared spectra of minerals and related inorganic compounds, Butterworth, London, 1975.
15. B.T. Poe, P.F. McMillan, and C. Angell, Al and Si coordination in $\text{SiO}_2\text{-Al}_2\text{O}_3$ glasses and liquids: A study by NMR and IR spectroscopy and MD simulations, *Chemical Geology*. Vol 96, No. 3-4, (1992), 333–349.
16. R. Devine, Ion implantation- and radiation-induced structural modifications in amorphous SiO_2 , *Journal of Non-Crystalline Solids*. Vol. 152, No. 1, (1993), 50–58.
17. S. Bordiga et al., Structure and Reactivity of Framework and Extraframework Iron in Fe-Silicalite as Investigated by Spectroscopic and Physicochemical Methods, *Journal of Catalysis*. Vol. 158, No. 2, (1996), 486–501.